

A Combined Experimental, Molecular Dynamics, DFT, NBO And AIM Analyses Of O–H···O Cyclic Dimer Model Of Hippuric Acid.

Jyoti Bhovi¹, J. R. Tonannavar¹, J. J. Tonannavar*¹

(Department Of Physics Karnatak University Dharwad, Karnataka, India, 580 003)

Abstract:

In the present work we report a study of the O–H···O cyclic dimer as determined by Molecular Dynamics Simulations for Hippuric acid. O–H···O bonded interaction is correlated to the unsymmetrical broad band structure observed in the experimental IR absorption spectrum from 3101 to 2958 cm⁻¹. To gain an understanding of the O–H···O cyclic dimer structure, we carried out MD simulations using 10 monomer species in TIP4P water solvent for 10ns time frame. We have identified different O–H···O and N–H···O bonds between carboxyl-carboxyl, carboxyl-carbonyl and carboxyl-amine groups in the linear dimer, cyclic dimer and trimer structures. Computed radial distribution function confirm the existence of O–H···O and N–H···O bonds and donor acceptor bond lengths in O–H···O and N–H···O bonds are less than the sum of van der Waals radii of O, N and H atoms. From the Density Functional Theory calculation, we considered the most stable cyclic dimer structure and optimized at B3LYP/6-311++G(d,p) level. Vibrational modes of the cyclic dimer are satisfactorily identified with the observed IR and Raman modes and frequency shift associated with the H-bonding. The charge transfer from the O lone pair orbital to the O-H anti-bonding orbital have been explained on the basis of Natural Bond Orbital (NBO) analysis. Further, Cyclic dimer structure has been characterized in terms of topological parameters using Bond Critical Point (BCP)s based on the Atoms In Molecules (AIM) theory. The attractive, van der Waals and repulsive interactions are explained by NCI method. Geometrical parameters, vibrational modes and other electronic properties of the cyclic dimer structure have shown to be a satisfactory model.

Key Word: Hippuric acid; Cyclic dimer; Molecular Dynamics; DFT; NCI analysis.

Date of Submission: 28-03-2025

Date of Acceptance: 08-04-2025

I. Introduction

Amino acids and their compounds play a significant role in the pharmaceutical industry. One such important amino acid is Hippuric acid, which was first discovered by Liebig¹. Hippuric acid is also known as N-benzoylglycine or benzoylaminoacetic acid (see Figure. 1). It is found in the urine of domestic animals and small amounts in human urine. Hippuric acid is differing from benzoic acid due to the presence of a nitrogen atom in its amide group, which contributes to its unique structure and properties. When benzoic acid is produced metabolically, it is rendered harmless through conjugation with the amino acid glycine to form Hippuric acid, which is then excreted. This metabolic reaction takes place in the liver. The conversion of benzoic acid to Hippuric acid can be used as a diagnostic test for liver function. If the liver is functioning properly, the benzoic acid will be efficiently converted to Hippuric acid and excreted². Among the amino acids whose structures have been determined through neutron diffraction and it is a distinctive molecule. Unlike N-acetylglycine, it does not exist as zwitterionic structure³. Hippuric acid contains a mono carboxylic group with three types of donor atoms: the nitrogen and oxygen atoms from the amide group, and the oxygen atoms from the carboxylic acid group. Hippuric acid molecules are found to be orthorhombic space group P2₁2₁2₁ with four molecules per unit cell of dimensions a=10.5, b=9.1 and c=8.8 Å⁴. The literature showed that the Hippuric acid molecule is potentially capable of forming H-bonds between carboxylic-carboxylic groups and carboxylic-amide groups⁵. Therefore, it is interest to investigate how the H-bonding facilitate the formation of different oligomer structures.

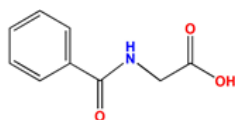


Figure 1: The molecular structure of Hippuric acid

Refat *et al* reported the XRD structure of Hippuric acid and its complexes with Mn(II), Au(III), and Zr(III)⁶. These complexes were synthesized and characterized using various analytical techniques, including elemental analysis, molar conductivity, magnetic measurements, spectral methods and simultaneous thermal analysis. This study suggests that the Hippuric acid molecule exhibits polymeric structures in both polar and non-polar solvents. This shows that the Hippuric acid molecule has the ability to form stable complexes with different metal ions, leading to the formation of polymeric structures. Karabacak *et al* studied the molecular structure, vibrational analysis and DFT analysis for monomer Hippuric acid⁷. Ringertz *et al* reported XRD structure of the Hippuric acid molecule, showing that it consist of two monomeric structures bound by O–H···O/N–H···O bonds⁸. Reflecting these structural characteristics, the experimental IR spectrum exhibits prominent signature vibrational bands, including a broad band ranging from 3101 to 2958 cm⁻¹, which indicates the presence of hydrogen bond interactions. We have been motivated by literature studies and IR experimental data to study the H-bonding interactions between Hippuric acid molecules. We performed MD and DFT calculations to study the structural features, vibrational and electronic characteristics of the Hippuric acid molecule. In the present work, we have performed the MD simulation over a 10 ns time scale to obtain different H-bonded oligomer structures. The functional groups of COOH, C=O and NH groups contributed to the formation of O–H···O and N–H···O bonds in linear dimer, trimer and cyclic dimer structures. The RDFs confirm the existence of H-bonds in all bonded structure obtained from MD simulation. Further, we considered the cyclic dimer structure, which is the most stable structure according to the Boltzmann population and binding energy analyses. We computed the most stable structure at B3LYP/6–311++G(d,p) level, which adequately matches the experimental IR band structure and are consistent with the Raman band characteristics. Electronic structure characterization, in terms of stabilization energies of the O–H···O bonds and topological parameters from AIM calculations has shown consistency with structural and vibrational properties. Additionally, we performed NCI analysis of the H-bonds to provide a detailed electronic characterization of the Hippuric acid molecule.

II. Material And Methods

Experimental Techniques

The powder sample of Hippuric acid purchased from MeRCK (formerly Sigma-Aldrich) and used as received without further purification. IR spectral measurement (4000-400cm⁻¹) was carried out on a Thermo-Fisher *Nicolet 6700* FT-IR spectrometer. The spectrometer consisted of Alum standard ETC Ever-Glo IR source, a standard interferometer bench and Deuterated Triglycine Sulphate (DTGS) detector. The samples were prepared using the KBr pellet method. Pellets were prepared of the sample-to-KBr in a 1:100 ratio and the spectra were recorded with 4cm⁻¹ resolution for 100 scans. Raman spectral measurements were performed on a *Bruker RFS27* stand-alone FT-Raman spectrometer module equipped with an Nd: YAG laser source, a standard interferometer and LN2 cooled-Ge detector. The spectra were measured in the range 4000–50 cm⁻¹ with 500 scans at spectral resolution of 2 cm⁻¹.

Computational Techniques

Determination of the stable monomer

In order to determine conformational flexibility of the monomer structure, we have performed a PES scan analysis at the RHF level of theory using the 3–21G basis set. The dihedral angles τ_1 and τ_2 are varied for the scan coordinates every 10°, and the molecular energy profile is calculated from 0 to 360°. Initially, the angle τ_1 was varied through N–C–C–O, here COOH group rotated around the CH₂ group (See Figure. 2(a)). As a result one minimum structure, M1 was observed with energy –625.361720 Hartree. Further, using the conformer M1, we varied the angle τ_2 (C–C–O–H), as a result stable minimum structure, M2 is predicted with energy–621.646002 Hartree (See Figure. 2(b)). Conformer M2 was optimized using the B3LYP/6–311++G(d,p) level. Frequency calculations confirmed the stability of this structure by showing no imaginary frequencies. This stable structure (M2) is used as the initial structure for the MD simulation.

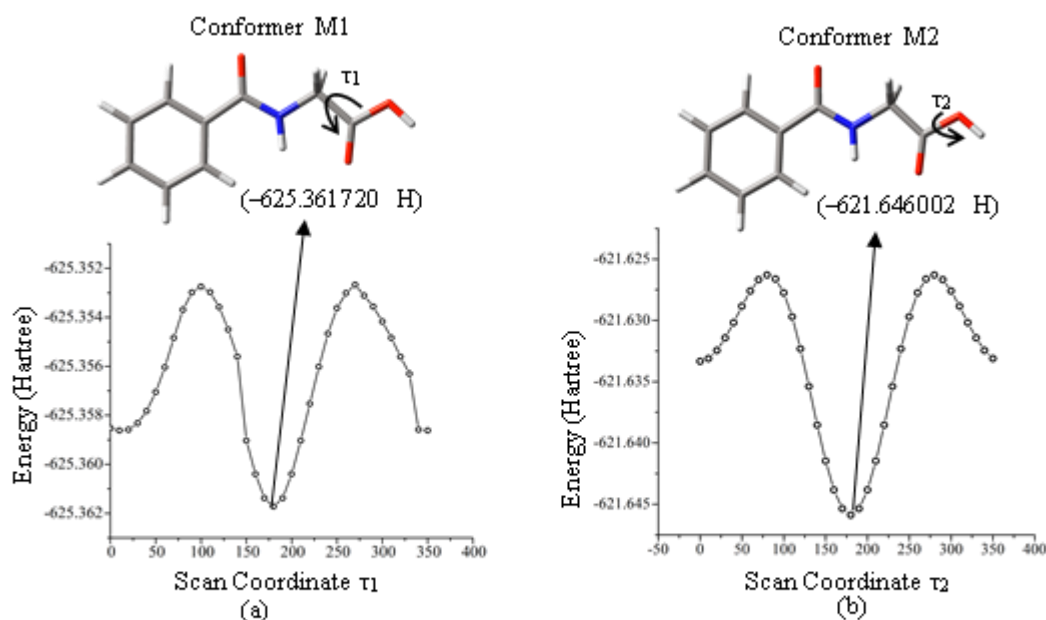


Figure 2: PES scan for the selected dihedral angles of τ_1 and τ_2 at RHF/3-21G level of Hippuric acid. The values in the brackets correspond to the energy of the stable conformer.

MD Methods

To study the *inter*-molecular interactions and stability of the oligomer structures of Hippuric acid, we have performed classical MD simulations. Initially, a triclinic box was defined with dimensions of 3.15, 2.64 and 2.73 nm for the simulation process. The optimized monomer structure, M2 (see Figure 3), was inserted into the system, followed by the addition of 10 monomers and 1000 TIP4P water molecules, resulting in a total density of the system is 1002.79 g/L. After defining the system, the simulation process begins with energy minimization process, so as to remove any close contacts between atoms.

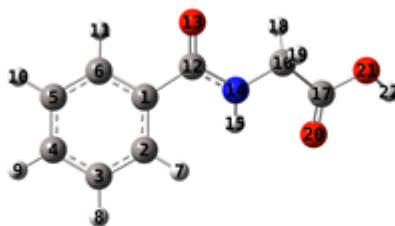


Figure 3: The optimized structure of Hippuric acid.

The algorithm used for energy minimization is steepest descent algorithm over 50,000 time steps. This is followed by equilibration phase-I, where a canonical ensemble (NVT) is run for 100 picoseconds at a temperature of 295 K, utilizing the Berendsen method for velocity rescaling and temperature control⁹. Further, equilibration phase-II consists of a 100 picoseconds isobaric-isothermal (NPT) simulation at a pressure of 1 atm and a temperature of 295 K, employing the Parainillo-Rahaman algorithm to achieve thermodynamic equilibrium¹⁰. Finally, after the system has equilibrated under constant temperature and pressure, MD production is carried out for a total of 10 ns. The snapshot of MD production simulation cell is shown in Figure 4. The partial atomic charges of the Hippuric acid monomer were computed using *CHELPG* based method as implemented in the *Gaussian 09W* suit and are presented in Table 1. The PME¹¹ method is used to calculate long-range potentials and the LINCS algorithm is used to constrain bonds involving hydrogen atoms.

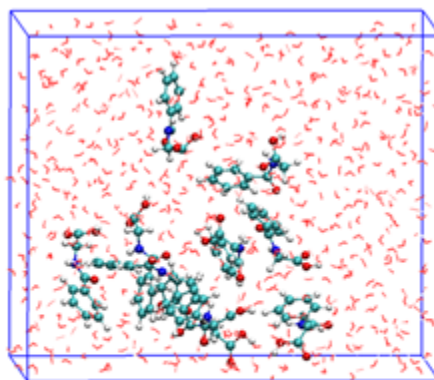


Figure 4: The snapshot shows the simulation box with the final MD production, containing Hippuric acid (in CPK model) and 1000 water molecules (in line models).

Table 1: OPLS-AA force fields, Partial charges, van der Waals and Lennard–Jones parameters of Hippuric acid.

| Atom types | | Atom | q(a.u)* | LJ-Parameters | |
|------------------|-------------|------|---------|-------------------------------|----------------------------------|
| | | | | $\sigma \times 10(\text{nm})$ | $\epsilon \times 10$ (kJ/mol) |
| Aromatic | C(OPLS_145) | C1 | 1.137 | 3.55 | 2.92 |
| | | C2 | -0.153 | 3.55 | 2.92 |
| | | C3 | -0.293 | 3.55 | 2.92 |
| | | C4 | -0.190 | 3.55 | 2.92 |
| | | C5 | -0.370 | 3.55 | 2.92 |
| | | C6 | -0.254 | 3.55 | 2.92 |
| | H(OPLS_146) | H7 | 0.159 | 2.42 | 1.25 |
| | | H8 | 0.166 | 2.42 | 1.25 |
| | | H9 | 0.161 | 2.42 | 1.25 |
| | | H10 | 0.167 | 2.42 | 1.25 |
| | | H11 | 0.206 | 2.42 | 1.25 |
| Carbonyl C=O | C(OPLS_235) | C12 | -0.805 | 3.75 | 4.39 |
| | O(OPLS_236) | O13 | -0.326 | 2.96 | 8.78 |
| N–H | N(OPLS_238) | N14 | -0.059 | 3.25 | 7.11 |
| | H(OPLS_241) | H15 | 0.236 | 0.00 | 0.00 |
| CH ₂ | C(OPLS_244) | C16 | -0.314 | 3.50 | 2.76 |
| | H(OPLS_140) | H18 | 0.243 | 2.50 | 1.25 |
| | | H19 | 0.243 | 2.50 | 1.25 |
| Carboxyl COOH | C(OPLS_267) | C17 | 0.207 | 3.75 | 4.39 |
| | O(OPLS_269) | O20 | -0.308 | 2.96 | 8.78 |
| | O(OPLS_268) | O21 | -0.147 | 3.00 | 7.11 |
| | H(OPLS_270) | H22 | 0.292 | 0.00 | 0.00 |

*– Partial charges obtained from B3LYP/6–311++G(d,p) method using *CHELPG* charges.

DFT Analysis

MD has been used for computing molecular clusters with H-bonds as characterized by radial distribution functions (RDFs). We performed MD calculations which yielded 3 types of *inter*–molecular O–H···O and 3 types of *inter*–molecular N–H···O bonds among COOH, NH and C=O moieties, as shown in Figure 5. To explicitly obtain structural information, all linear dimer and trimer structures were optimized at the B3LYP/6–311++G (d, p) level. To search for the local minimum of O–H···O cyclic dimer structure, we performed frequency calculations at the same level and selected the structure as per the convergence criterion of

no imaginary vibrational frequencies. We computed potential energy distributions (PED) for the all IR and Raman modes using *VEDA* program. NBO analysis as implemented in the *Gaussian 09W* was used to study the electronic charge delocalization and stabilization energies computed from the interaction matrix elements in the second order perturbation theory. The O-H...O bonds and bond strengths through bond critical points (BCP), isosurfaces to map different interactions from AIM and NCI as implemented in *Multifn* and *VMD* software packages were also computed.

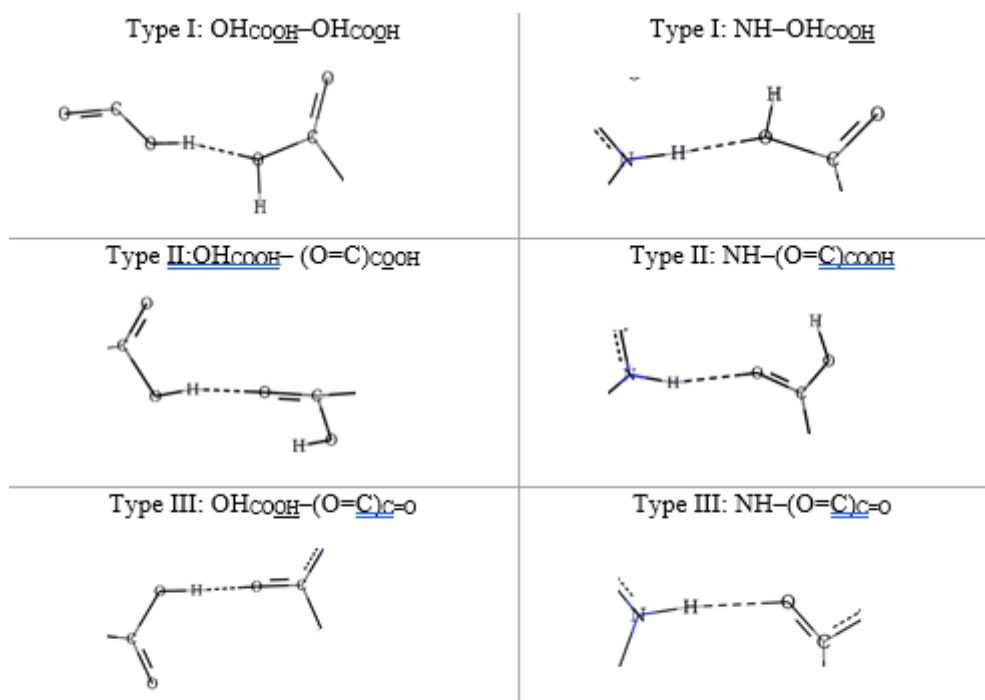


Figure 5: Possible *inter*-molecular hydrogen bonds of Hippuric acid molecules between COOH, NH and C=O moieties, predicted through MD simulation. Underlined subscripts indicate atoms involved in hydrogen bonds (Left: O-H...O bonds, Right: N-H...O bonds).

III. Results And Discussion

MD Analysis

H-bond Analysis

We computed average number of O-H...O and N-H...O bonds and their lifetime (τ) are given in Table 2. The formation of H-bonds between COOH and the C=O group (Type III) predicts the maximum number of H-bonds in comparison to all other H-bonds and also, it has the longest lifetime of 35.22 ps. And H-bonds between solvent (water) and Hippuric acid are also computed and are found not so strong and life time is also less compared to Hippuric acid-Hippuric acid *inter*-molecular O-H...O/N-H...O bonds.

Table 2: Computed average number of H-bonds and life time of O-H...O/N-H...O bonds.

| Types of H-bonds | | | Average number of H-bonds(HBs) | Life time (τ) in ps |
|------------------|----------|--|--------------------------------|----------------------------|
| O-H...O | Type I | O-H _{<u>COOH</u>} ...O _{<u>COOH</u>} | 0.184 | 12.80 |
| | Type II | O-H _{<u>COOH</u>} ...O _{<u>COOH</u>} | 0.329 | 25.81 |
| | Type III | O-H _{<u>COOH</u>} ...O _{<u>C=O</u>} | 0.767 | 35.22 |
| N-H...O | Type I | N-H...O _{<u>COOH</u>} | 0.174 | 07.09 |
| | Type II | N-H...O _{<u>COOH</u>} | 0.264 | 10.88 |
| | Type III | N-H...O _{<u>C=O</u>} | 0.298 | 08.88 |

Note-Bold and underline atoms refer to those involved in the H-bond interaction.

Radial Distribution Function (RDF) Analysis

The RDF curves are analyzed for the bonded molecules to examine the H-bonds in the dynamic process. To characterize the O-H...O and N-H...O bond interactions in various structures, the site-site RDFs (H...O) of all the 6 hydrogen bonds were evaluated, as shown in Figure 6. In Figure 6(a), a prominent first peak appears at 1.7 Å in the RDF curve, indicating a strong interaction between the O-H in COOH group and the O

atom in the C=O group (Type III O–H···O bond). This first shell suggests that O–H atomic pairs are surrounded by ~ 6.4 O atoms, resulting in a coordination number (CN) of first shell ~ 6.4. Figures (b) and (c) further illustrate the presence of H–bonding between the COOH···O=C=O (Type II O–H···O bond) and COOH···COOH (Type I O–H···O bond) groups, with first peaks at 2.2 and 1.4 Å respectively. In Figure (d), the sharp peak at 2.2 Å strongly indicates the presence of H–bonds between NH and C=O (Type III N–H···O bond) groups, resulting in a first-shell coordination number ~7. This suggests that each N–H pair interacts with approximately 7 O atoms. Similarly, Figures (e) and (f) further illustrate the presence of H–bonding between the NH···O=C=O (Type II N–H···O bond) and NH···COOH (Type I N–H···O bond) groups, showing first peaks at 2.4 and 2.1 Å respectively. The coordination numbers for the first shell of all RDFs are given in Table 3. Geometrical criterion used for all H-bonds existence between hydrogen (H) and acceptor (A) is given by the condition $r < r^c$, where r^c is the cut-off values for the Hydrogen-Acceptor distance, specifically 2.72 Å¹². The cut-off values for the *inter*-molecular H···O distances are based on the first minimum of the corresponding RDFs. All calculated RDFs for H···O bond distances in O–H···O and N–H···O bonds, are less than the cut-off value r^c (In the Figure 6, the straight line indicates the cut-off value of r^c). This analysis confirms that stable H–bonds exist between the O/N (donor) atoms and the O (acceptor) atom, satisfying the van der Waals criteria.

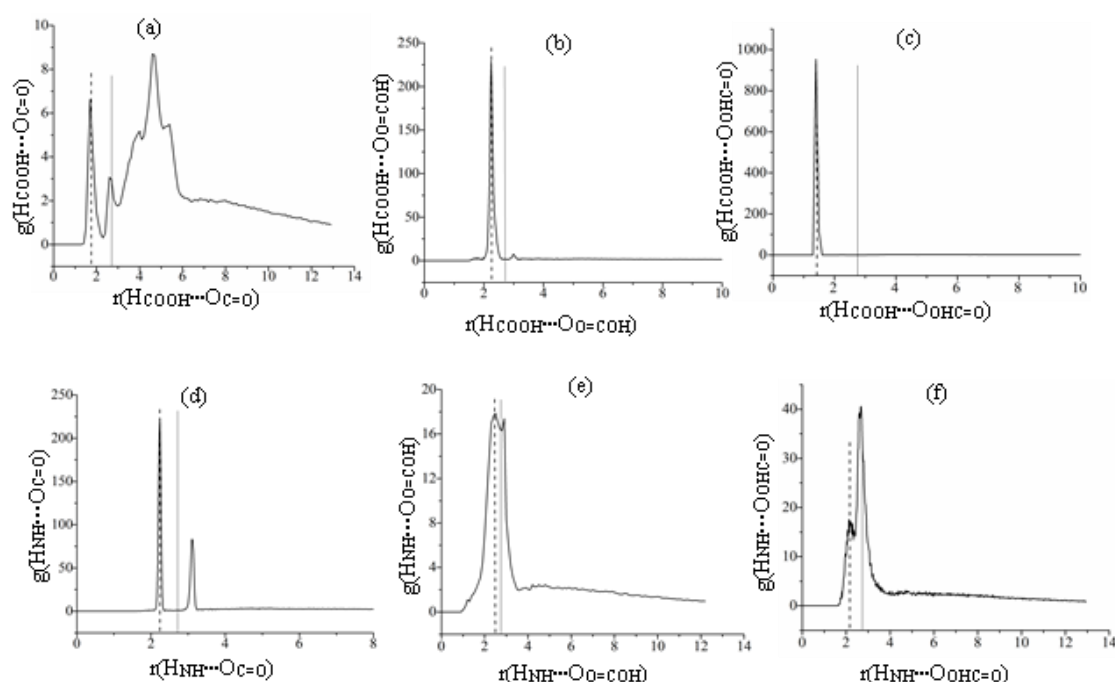


Figure 6: The radial distribution functions of the upper figures represent the interactions between COOH and C=O, as well as between COOH and COOH moieties, while the lower RDF illustrates the interactions between NH and C=O, and COOH. Note: Dotted line indicates the existence of H···O bond and straight line indicates the cut-off value of H···O distance.

Table 3: Coordination numbers from the first peak of radial distribution functions for different atomic pairs.

| Sl No. | H-bonds | Coordination number |
|--------|---------------------------------|---------------------|
| 1 | $(O-H)_{COOH} \cdots O_{C=O}$ | 9.3 |
| 2 | $(O-H)_{COOH} \cdots O_{O=COH}$ | 9.9 |
| 3 | $(O-H)_{COOH} \cdots O_{OHC=O}$ | 7.1 |
| 4 | $N-H \cdots O_{C=O}$ | 9.9 |
| 5 | $N-H \cdots O_{O=COH}$ | 10 |
| 6 | $N-H \cdots O_{OHC=O}$ | 9.9 |

DFT Structural Analysis

Following the MD simulation, it generated linear dimer (LD1, LD2, LD3, LD4, LD5 and LD6), cyclic dimer (CD1, CD2 and CD3) and trimer (Tr1, Tr2, Tr3, Tr4, Tr5, Tr6, Tr7 and Tr8) structures. Further, all predicted structures were used in geometry optimization at the B3LYP/3–21G level. The counterpoise calculations were carried out to get complexation energy (binding energy) for all these structures at the same level. The Boltzmann populations were calculated by considering Gibbs free energies. The Gibbs free energies, Boltzmann population and binding energies for these structures are presented in Table 4.

Table 4: Calculated Gibbs free energies, Boltzmann population and binding energies for linear dimer, cyclic dimer and trimer structures at the B3LYP/3–21G level.

| Types of Structures | | Gibbs free energy (Hartree) | Population (%) | E _B kcal/mol |
|---------------------|-----------------------------------|-----------------------------|-----------------------|-------------------------|
| Linear Dimer | LD1: N36–H37···O21 | –1250.76036 | 1.76x ⁻⁵ | –19.90 |
| | LD2: N14–H15···O35 | –1250.75963 | 8.18x10 ⁻⁶ | –9.62 |
| | LD3: O43–H44···O20 | –1250.75743 | 1.01x10 ⁻⁷ | –11.64 |
| | LD4: O43–H44···O13 | –1250.75538 | 6.11x ⁻⁸ | –17.10 |
| | LD5: O43–H44···O21 | –1250.75498 | 0.00 | –30.44 |
| | LD6: N14–H15···O42 | –1250.74310 | 0.00 | –6.83 |
| Cyclic Dimer | CD1: O21–H22···O42;O43–H44···O20 | –1250.77513 | 99.99997 | –24.11 |
| | CD2: N14–H15···O42;N36–H37···O20 | –1250.75258 | 8.06x10 ⁻⁷ | –5.91 |
| | CD3: N14–H15···O42;O43–H44···O21 | –1250.75546 | 9.03x10 ⁻⁸ | –17.04 |
| Trimer | Tr1: O21–H22···O64;O43–H44···O13 | –1876.17167 | 99.65 | –53.42 |
| | Tr2: N36–H37···O13;O65–H66···O42 | –1876.16628 | 0.34 | –33.47 |
| | Tr3: O65–H66···O13;O21–H22···O35 | –1876.16201 | 0.003 | –29.23 |
| | Tr4: O21–H22···O57;N58–H59···O35 | –1876.16109 | 0.0014 | –30.81 |
| | Tr5: O21–H22···O65;O65–H66···O35 | –1876.15969 | 0.0003 | –33.05 |
| | Tr6: O21–H22···O57;O43–H44···O65 | –1876.15586 | 5.8X10 ⁻⁶ | –21.31 |
| | Tr7: N36–H37···O21; O43–H44···O65 | –1876.15343 | 4.5X10 ⁻⁷ | –29.10 |
| | Tr8: O21–H22···O35;O65–H66···O13 | –1876.15017 | 1.49X10 ⁻⁸ | –29.54 |

Based on the Boltzmann population and binding energy analysis, the cyclic dimer structure (CD1), having 99.99% population among all dimer and trimer structures, was considered as the most stable cyclic dimer structure for further vibrational and electronic structure calculations.

Structure Analysis of Cyclic Dimer (CD1)

The most stable cyclic dimer, (CD1) structure is considered for optimization and frequency calculation at B3LYP/6–311++G(d,p) level. Figure 7 illustrates the optimized structure of CD1. The optimized geometrical bond lengths and bond angles and H–bonding parameters are given in Table 5. These are compared with the experimental XRD results² of the monomer Hippuric acid. In CD1 structure, the ring C–C bond lengths exhibit a narrow range from 1.390 to 1.400 Å. The C–C bond lengths show minor changes from the XRD data with deviations from 0.07 to 1.01%. Similarly, the free C=O (C12–O13 and C34–O35) bond lengths exhibit a value of 1.224 Å, which is shorter than the corresponding value observed in the XRD data with deviation of 1.05%. The CD1 exhibits O–H···O bonds (O21–H22···O42 and O43–H44···O20) between carboxylic groups with a local center of inversion. The CD1 structure induces a slight elongation of the O21–H22 and O43–H44 bonds, both increasing from 0.990 Å in the XRD data to 1.003 Å, resulting in a deviation of 0.013 Å. Moreover, the calculated *inter*–molecular H···O distances for both O–H···O bonds are 1.646 Å and O···O distances are 2.649 Å. The O···O bond lengths are considerably smaller than those observed in the XRD structure data.

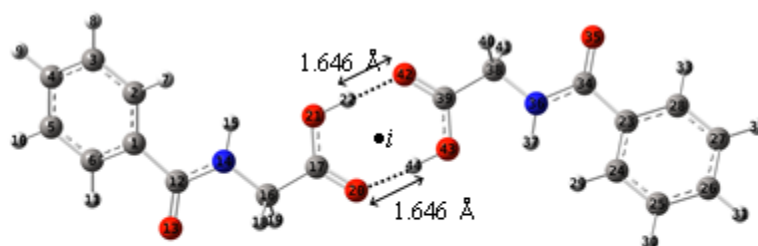


Figure 7: Optimized cyclic dimer (CD1) structure of Hippuric acid, computed at B3LYP/6–311++G(d,p) level. (*i*-denotes the local center of inversion).
Carbon- ; Oxygen- ; Nitrogen- ; Hydrogen-

Table 5: Computed bond lengths and bond angles of cyclic dimer (CD1) structure of Hippuric acid calculated at the B3LYP/6–311++G(d,p) level and compared with XRD data.

| Bond lengths (Å) | | | | |
|--|-------|-------------|-------|----------|
| Parameters | CD1 | Parameters | CD1 | XRD* |
| C1–C2 | 1.400 | C23–C24 | 1.400 | 1.402 |
| C2–C3 | 1.393 | C24–C25 | 1.393 | 1.402 |
| C3–C4 | 1.393 | C25–C26 | 1.393 | 1.392 |
| C4–C5 | 1.395 | C26–C27 | 1.395 | 1.381 |
| C5–C6 | 1.390 | C27–C28 | 1.390 | 1.388 |
| C6–C1 | 1.399 | C28–C23 | 1.399 | 1.389 |
| C2–H7 | 1.084 | C24–H29 | 1.084 | 1.076 |
| C3–H8 | 1.084 | C25–H30 | 1.084 | 1.105 |
| C4–H9 | 1.084 | C26–H31 | 1.084 | 1.102 |
| C5–H10 | 1.084 | C27–H32 | 1.084 | 1.088 |
| C6–H11 | 1.082 | C28–H33 | 1.082 | 1.106 |
| C1–C12 | 1.502 | C23–C34 | 1.502 | 1.499 |
| C12–O13 | 1.224 | C34–O35 | 1.224 | 1.237 |
| C12–N14 | 1.367 | C34–N36 | 1.367 | 1.342 |
| N14–H15 | 1.007 | N36–H37 | 1.007 | 0.997 |
| N14–C16 | 1.447 | N36–C38 | 1.447 | 1.446 |
| C16–H18 | 1.094 | C38–H40 | 1.094 | 1.073 |
| C16–H19 | 1.096 | C38–H41 | 1.096 | 1.106 |
| C16–C17 | 1.509 | C38–C39 | 1.509 | 1.506 |
| C17–O20 | 1.224 | C39–O42 | 1.224 | 1.204 |
| C17–O21 | 1.319 | C39–O43 | 1.319 | 1.301 |
| O21–H22 | 1.003 | O43–H44 | 1.003 | 0.990 |
| Bond angles (°) | | | | |
| C2–C1–C6 | 119.2 | C24–C23–C28 | 119.2 | 119.9 |
| C2–C1–C12 | 123.4 | C24–C23–C34 | 123.4 | 122.5 |
| C6–C1–C12 | 117.3 | C28–C23–C34 | 117.3 | 117.6 |
| C1–C2–C3 | 120.3 | C23–C24–C25 | 120.3 | 119.3 |
| C1–C2–H7 | 120.7 | C23–C24–H29 | 120.7 | 121.9 |
| C3–C2–H7 | 118.8 | C25–C24–H29 | 118.8 | 118.9 |
| C2–C3–C4 | 120.0 | C24–C25–C26 | 120.0 | 120.0 |
| C2–C3–H8 | 119.7 | C24–C25–H30 | 119.8 | 119.6 |
| C4–C3–H8 | 120.1 | C26–C25–H30 | 120.1 | 120.4 |
| C3–C4–C5 | 119.8 | C25–C26–C27 | 119.8 | 120.4 |
| C3–C4–H9 | 120.0 | C25–C26–H31 | 120.0 | 118.6 |
| C5–C4–H9 | 120.1 | C27–C26–H31 | 120.1 | 121.1 |
| C4–C5–C6 | 120.1 | C26–C27–C28 | 120.1 | 120.1 |
| C4–C5–H10 | 120.0 | C26–C27–H32 | 120.0 | 118.3 |
| C6–C5–H10 | 119.8 | C28–C27–H32 | 119.8 | 121.6 |
| C1–C6–C5 | 120.3 | C23–C28–C27 | 120.3 | 120.4 |
| C1–C6–H11 | 118.4 | C23–C28–H33 | 118.4 | 118.5 |
| C5–C6–H11 | 121.1 | C27–C28–H33 | 121.1 | 121.5 |
| C1–C12–O13 | 122.1 | C23–C34–O35 | 122.1 | 119.7 |
| C1–C12–N14 | 116.5 | C23–C34–N36 | 116.5 | 118.5 |
| O13–C12–N14 | 121.2 | O35–C34–N36 | 121.2 | 121.9 |
| C12–N14–H15 | 121.0 | C34–N36–H37 | 121.0 | 121.1 |
| C12–N14–C16 | 120.0 | C34–N36–C38 | 120.0 | 121.3 |
| H15–N14–C16 | 117.7 | H37–N36–C38 | 117.7 | 117.5 |
| N14–C16–C17 | 113.3 | N36–C38–C39 | 113.3 | 114.0 |
| N14–C16–H18 | 111.0 | N36–C38–H40 | 111.0 | 108.5 |
| N14–C16–H19 | 111.4 | N36–C38–H41 | 111.4 | 110.4 |
| C17–C16–H18 | 107.6 | C39–C38–H40 | 107.6 | 109.0 |
| C17–C16–H19 | 107.3 | C39–C38–H41 | 107.3 | 105.9 |
| H18–C16–H19 | 105.5 | H40–C38–H41 | 105.5 | 108.9 |
| C16–C17–O20 | 120.8 | C38–C39–O42 | 120.8 | 125.7 |
| C16–C17–O21 | 114.9 | C38–C39–O43 | 114.9 | 110.4 |
| O20–C17–O21 | 124.1 | O42–C39–O43 | 124.2 | 123.8 |
| C17–O21–H22 | 110.8 | C39–O43–H44 | 110.8 | 113.6 |
| H-bonded Parameters (Å) and angle (°) of CD1 | | | | |
| D–H...A | D–H | H...A | D–A | ∠D–H...A |
| O21–H22...O42 | 1.003 | 1.646 | 2.649 | 178.0 |
| O43–H44...O20 | 1.003 | 1.646 | 2.649 | 178.0 |

Vibrational Analysis

Vibrational analysis was performed on the optimized structure of CD1 frequency calculations at B3LYP/6–311++G(d,p) level. The CD1 structure consists of 44 atoms, exhibits 126 normal modes of

vibrations. The experimental IR and Raman spectra of Hippuric acid were compared with the simulated spectrum of CD1 as shown in Figure 8 and 9. Table 6 provides the comprehensive assignment of the experimental IR, Raman and simulated CD1 vibrational modes along with their PED contributions. To improve the agreement of the simulated data with experimental data, the calculated wavenumbers were uniformly scaled by a factor of 0.9688. The theoretical approach accurately replicated the experimental data after using a uniform scaling factor. Generally, the intense peak observed in the region 3500–3300 cm^{-1} is assigned to N–H stretching vibration¹³. The observed IR band at 3342 cm^{-1} is attributed to the N–H stretching vibration. The corresponding computed N–H stretching vibrations are predicted at 3528 cm^{-1} for each monomer in CD1 structure. In the IR spectrum, broad region from 3101 to 2958 cm^{-1} exhibits overlapping contributions from bonded O–H and ring C–H stretching vibrations. A broad unsymmetrical band structure with peak at 3079 cm^{-1} , accompanied by multiple shoulders is assigned to bonded O–H and ring C–H stretching vibrations. The computed O–H bonded frequencies are accurately predicted at 3050 and 2946 cm^{-1} for the CD1 structure. The free O–H stretching vibration of the monomer is predicted at 3643 cm^{-1} , with a relative downshift of 16% for the bonded O–H frequency. The CD1 structure is formed by two monomers are in a head to–tail configuration, forming a local center of inversion. This symmetry has caused the occurrence of two bands in a mutually exclusive manner^{14,15,16}. The two mutual exclusive bands, one IR band at 1758 cm^{-1} and one very weak Raman band at 1733 cm^{-1} due to local center of inversion formed by the cyclic H–bonding. These bands are assigned to bonded C=O stretching vibrations, computed at 1712 and 1660 cm^{-1} . Additionally, two free C=O symmetric and asymmetric stretching modes predicted at 1668 cm^{-1} from each monomer. The in–plane O–H bending modes were calculated at 1422 and 1403 cm^{-1} and the corresponding medium intensity IR band observed at 1415 cm^{-1} and weak Raman band observed at 1416 cm^{-1} . A band of medium to strong intensity in the region 960–875 cm^{-1} is due to the out of plane deformation of carboxylic group O–H···O bonding. The out of plane O–H bending mode was calculated at 927 cm^{-1} , these O–H deformation bands observed at 943 and 941 cm^{-1} in IR and Raman spectra respectively^{17,18}. The broad band extending from 2700 to 2500 cm^{-1} , with distinctive shoulders of decreasing intensity corresponds to combination bands. The weak to medium combination bands observed at 2689, 2603, 2568 and 2478 cm^{-1} arise due to the O–H···O bonding, as assignments in Table 6. These combination bands are characteristic of carboxyl dimers and due to combination of the 1300 and 1420 cm^{-1} band due to interacting C–O stretching and O–H in plane deformation vibration¹³.

The CH stretching vibrations of CH₂ groups are less intense resolved bands between 2900 and 2700 cm^{-1} in IR spectra and these are attributed to hydrogen bonding interactions. The corresponding Raman bands are observed at 2984 and 2940 cm^{-1} . The computed symmetric and asymmetric CH stretching bands are located at 2969 and 2937 cm^{-1} respectively. The CH₂ scissoring mode produces a characteristic band near 1442 cm^{-1} and this mode is observed at 1445 cm^{-1} in both the IR and Raman spectra. Similarly, the CH₂ wagging mode is predicted at 1321 cm^{-1} and corresponding IR and Raman bands are observed at 1334 and 1336 cm^{-1} respectively. Strong characteristic bands corresponding to ring C–C vibrations are observed at 1602 cm^{-1} in both the IR and Raman spectra. The computed values for these vibrations are 1590 and 1568 cm^{-1} , with a deviation of less than 2.1%. The ring C–H stretching mode is observed at 3072 cm^{-1} in the Raman spectrum. Computed values for this mode in the CD1 structure are 3101, 3090, 3081, and 3071 cm^{-1} , showing a close match with experimental data. The characteristic breathing mode of the aromatic ring is observed at 999 cm^{-1} in both IR and Raman spectra. The corresponding C–C bending mode is calculated at 984 cm^{-1} . The C–H in–plane ring bending vibrations, coupled with C–C stretching modes, appear as a number of sharp bands in the region 1300–1000 cm^{-1} . The C–N bending vibration is observed at 1488 cm^{-1} IR spectrum. The computed value is 1491 cm^{-1} , with a deviation of less than 1% showing good agreement between theoretical and experimental data. In the lower region, the weak H···O bond exhibits calculated band of 101 cm^{-1} , this band corresponds well with a strong Raman band observed at 100 cm^{-1} . Overall, all assignments demonstrate good agreement with both experimental and theoretical data.

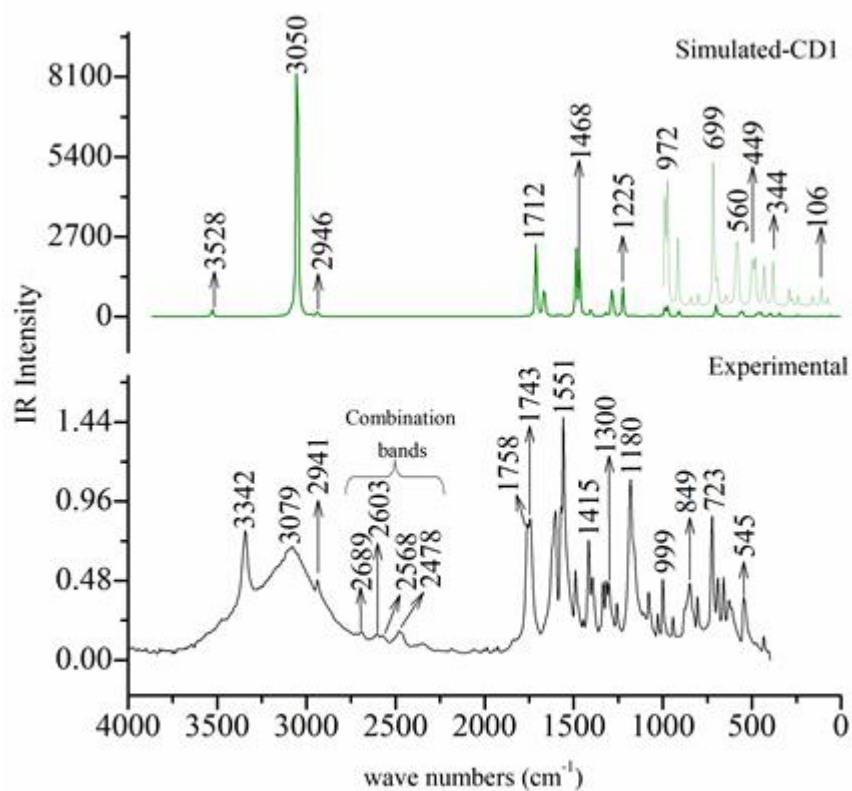


Figure 8: Experimental IR spectrum of Hippuric acid is compared with simulated spectrum of cyclic dimer structure.

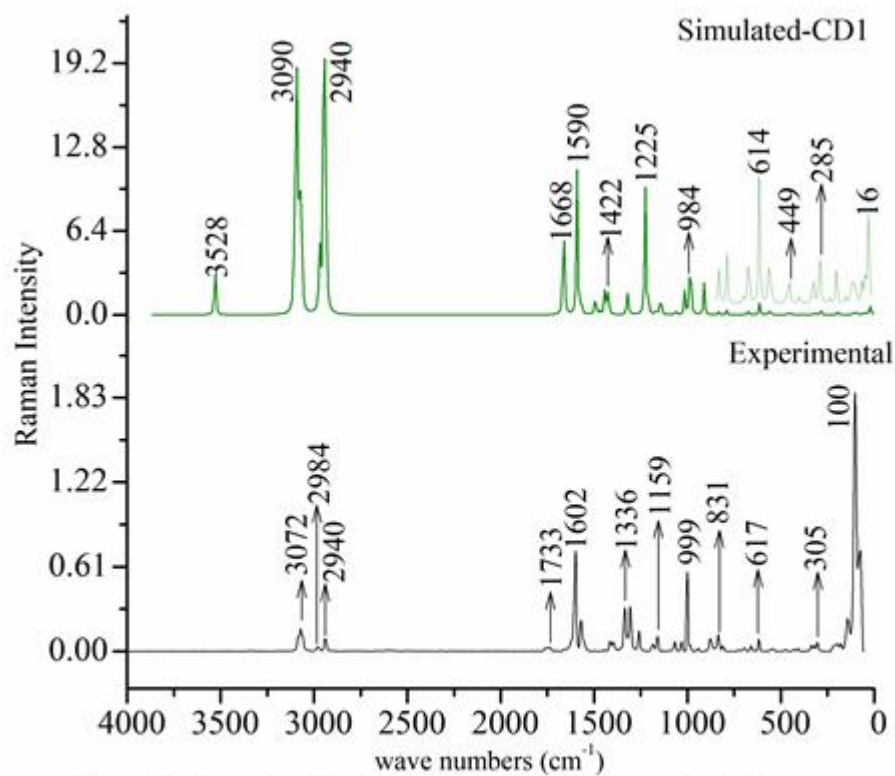


Figure 9: Experimental Raman spectrum of Hippuric acid is compared with simulated spectrum of cyclic dimer structure.

Table 6: Computed vibrational frequencies (cm⁻¹) of monomer and cyclic dimer (CD1) of Hippuric acid compared with experimental data.

| Experimental ^a | | Theoretical ^b | | Assignments ^c (PED %) |
|---------------------------|--------|--------------------------|------------|---|
| IR | Raman | Monomer | CD1 | |
| – | – | 3643 | – | ν_s OH[100] |
| 3342s | – | 3500 | 3528, 3528 | ν_s NH[77] + ν_s NH[23] |
| – | – | 3102 | 3101, 3101 | ν_{as} CH[58] + ν_s CH[28] |
| – | – | 3091 | 3090, 3090 | ν_{as} CH[21] + ν_s CH[21] + ν_{as} CH[17] + ν_s CH[17] |
| 3079b | – | 3081 | 3081, 3081 | ν_{as} CH[38] + ν_s CH[28] + ν_{as} CH[18] + ν_s CH[11] |
| – | 3072m | 3072 | 3071, 3071 | ν_{as} CH[34] + ν_{as} CH[31] + ν_{as} CH[25] |
| – | – | 3065 | 3064, 3064 | ν_{as} CH[19] + ν_{as} OH[19] + ν_{as} CH[16] + ν_{as} CH[16] + ν_{as} CH[11] + ν_{as} CH[10] |
| – | – | – | 3050 | Bonded OH [O21-H22...O42] |
| – | 2984vw | – | 2969 | ν_{as} CH[55] + ν_{as} CH[35] |
| – | – | 2962 | 2969 | ν_s CH[54] + ν_s CH[35] |
| – | – | – | 2946 | Bonded OH [O43-H44...O20] |
| 2941w | 2940w | 2940 | 2937 | ν_s CH[48] + ν_s CH[41] |
| 2689w | – | – | – | 1424 [β HOC + β COH + ν_s OC + ν_s OC] + 1139 [ν_s NC + ν_s NC] |
| 2603w | – | – | – | 1668 [ν_s OC + ν_s OC] + 927 [τ OHOC + τ COHO + τ HOCC + τ CCOH] |
| 2568w | – | – | – | 1310 [β HCC + β HCC + β HCC + β HCC] + 1209 [β HCC + β HCC + τ HCCO + τ HCCO] |
| 2478m | – | – | – | 1286 [ν_s OC + ν_s OC + β HOC] + 1209 [β HCC + β HCC + τ HCCO + τ HCCO] |
| 1758s | – | 1754 | 1712 | ν_s OC[40] + ν_s OC[39] bonded in CD1 |
| – | 1733vw | 1662 | 1668, 1668 | ν_s OC[39] + ν_s OC[38] |
| – | – | – | 1660 | ν_s OC[33] + ν_s OC[31] bonded in CD1 |
| 1602s | 1602s | 1590 | 1590, 1590 | ν CC[16] + ν CC[12] |
| 1572sh | – | 1569 | – | β HCC[23] + β HCC[14] |
| 1551vs | 1568m | – | 1568, 1568 | ν CC[24] + ν CC[18] |
| 1488m | – | 1491 | 1491 | β HNC[19] + β HNC[19] |
| 1445w | 1445vw | – | 1442, 1442 | β HCH[21] + β HCH[21] |
| 1415m | 1416w | – | 1422 | β HOC [21] + β OHO[10] |
| 1393m | 1398w | – | 1407 | ν OC[10] + ν OC[10] + β HOC[26] + β COH[23] |
| 1334m | 1336m | – | – | τ HCCO [52] + β HCC[14] |
| 1317m | – | – | 1321 | β HCH[16] + β HCH[16] |
| 1300m | 1303m | 1292 | 1291 | ν_s CC[16] + ν_s CC[12] |
| 1258w | 1256w | 1274 | 1272 | ν_s OC[23] + ν_s OC[21] |
| 1180s | 1184vw | 1199 | 1209, 1209 | β HCC[27] + β HCC[25] + τ HCCO [14] + τ HCCO [13] |
| – | 1159w | 1151 | 1147 | β HCC[57] + ν CC[16] |
| 1079m | – | 1073 | 1077 | β HCC[64] + ν CC[26] |
| – | 1066w | 1057 | 1062, 1062 | ν_s NC[38] + β CCC[12] |
| 1028w | 1031w | 1015 | 1014, 1014 | ν_s CC[12] + ν_s CC[11] |
| 999m | 999s | – | 989 | τ COHO [21] + τ CCOH [16] + τ OHOC [14] |
| 943w | 941vw | – | 927 | τ OHOC[33] + τ COHO[30] + τ HOCC[13] + τ CCOH[13] |
| 849m | 876w | – | – | ν CC[46] |
| – | 831w | 832 | 833 | τ HCCC [15] + τ HCCC [15] + τ HCCC [15] + τ HCCC [15] + τ HCCC [10] |
| 804m | 809w | 791 | 789, 788 | γ ONCC [22] + γ ONCC [17] |
| 723s | – | – | – | γ ONCC [31] + τ HCCC [25] + τ CCCC [11] |
| 691m | 694vw | 699 | 699, 699 | τ HCCC[29] + τ CCCC[42] |
| 660m | 657vw | 666 | 670 | β CCC [17] + β CCC [17] |
| 628w | – | 629 | 623 | β OCO [14] + β OCO [24] |
| – | 617w | 613 | 614 | β OCO [22] + β OCO [30] |
| 545m | – | – | 550 | γ OCOC [17] + γ OCOC [21] |
| 434w | – | 448 | 449 | τ HNCC [28] + τ HNCC [29] |
| – | 337w | – | 321 | β OCN[10] + β OCN [10] |
| – | 305w | – | 285 | ν OH [24] |
| – | 198w | – | 194 | τ CCCC [14] + τ CCNC [15] + τ CNCC [15] |
| – | 141sh | – | 142 | β OHO [16] + β COH [19] |
| – | 100vs | – | 101 | ν OH [44] + β HOC [13] |

Note: ^a – Letters vs, s, m, w, vw, b and sh are used as very strong, strong, medium, weak, very weak, broad and shoulder respectively.
^b – Frequencies are scaled by 0.9688.
^c – All assignments refer to the cyclic dimer frequencies. The Greek symbols used in the table ν , β , τ and γ refer to stretching, bending, torsion and out of plane bending respectively. The subscript of stretching vibrations are defined as as-antisymmetric and s-symmetric stretching.

NBO Analysis

NBO analysis provides an efficient method for interpreting *intra*- and *inter*-molecular H-bonding and charge transfer in both filled and unfilled orbitals of CD1 structure^{19,20}. The second order perturbation energies, E⁽²⁾ represent strength of interactions between donor and acceptor orbitals of hydrogen bonds. Table 7 presents the *intra*- and *inter*-molecular interactions of donor-acceptor NBO pairs of CD1 structure. Figure 10 represents the graphical electron orbital maps of the NBOs corresponding to O–H...O interactions for CD1. The *inter*-

molecular interactions are formed by the orbital overlap between interacting $n_2(\text{O}20) \rightarrow \sigma_1^*(\text{O}43\text{--H}44)$ NBOs and $n_2(\text{O}42) \rightarrow \sigma_1^*(\text{O}21\text{--H}22)$ NBOs, which have the stabilization energies, $E^{(2)}$ values of 22.57 and 22.58 kcal/mol respectively. The identical values of $E^{(2)}$ suggest that the cyclic hydrogen bonding in CD1 is having local symmetry. The larger $E^{(2)}$ value represents a stronger interaction between electron donor and electron acceptor pairs. The *intra*-bond forms between $n_1(\text{O}21) \rightarrow \sigma_1^*(\text{N}14\text{--H}15)$ and $n_1(\text{O}43) \rightarrow \sigma_1^*(\text{N}36\text{--H}37)$ with stabilization energy value of, $E^{(2)} = 0.91$ kcal/mol.

Table 7: Second-order perturbation theory analysis of Fock Matrix in the NBO basis for the *intra*- and *inter* H-bonding interactions in cyclic dimer (CD1) structure of Hippuric acid.

| Types of Structures | Types of bonding | Donor NBO Ω_i | Acceptor NBO Ω_{ij} | $E^{(2)}$ (kcal/mol) |
|---------------------|------------------|----------------------|--------------------------------------|----------------------|
| Cyclic dimer | <i>Intra</i> | $n_1(\text{O}21)$ | $\sigma_1^*(\text{N}14\text{--H}15)$ | 0.91 |
| | | $n_1(\text{O}43)$ | $\sigma_1^*(\text{N}36\text{--H}37)$ | 0.91 |
| | <i>Inter</i> | $n_1(\text{O}20)$ | $\sigma_1^*(\text{O}43\text{--H}44)$ | 9.37 |
| | | $n_2(\text{O}20)$ | $\sigma_1^*(\text{O}43\text{--H}44)$ | 22.57 |
| | | $n_1(\text{O}42)$ | $\sigma_1^*(\text{O}21\text{--H}22)$ | 9.37 |
| | | $n_2(\text{O}42)$ | $\sigma_1^*(\text{O}21\text{--H}22)$ | 22.58 |

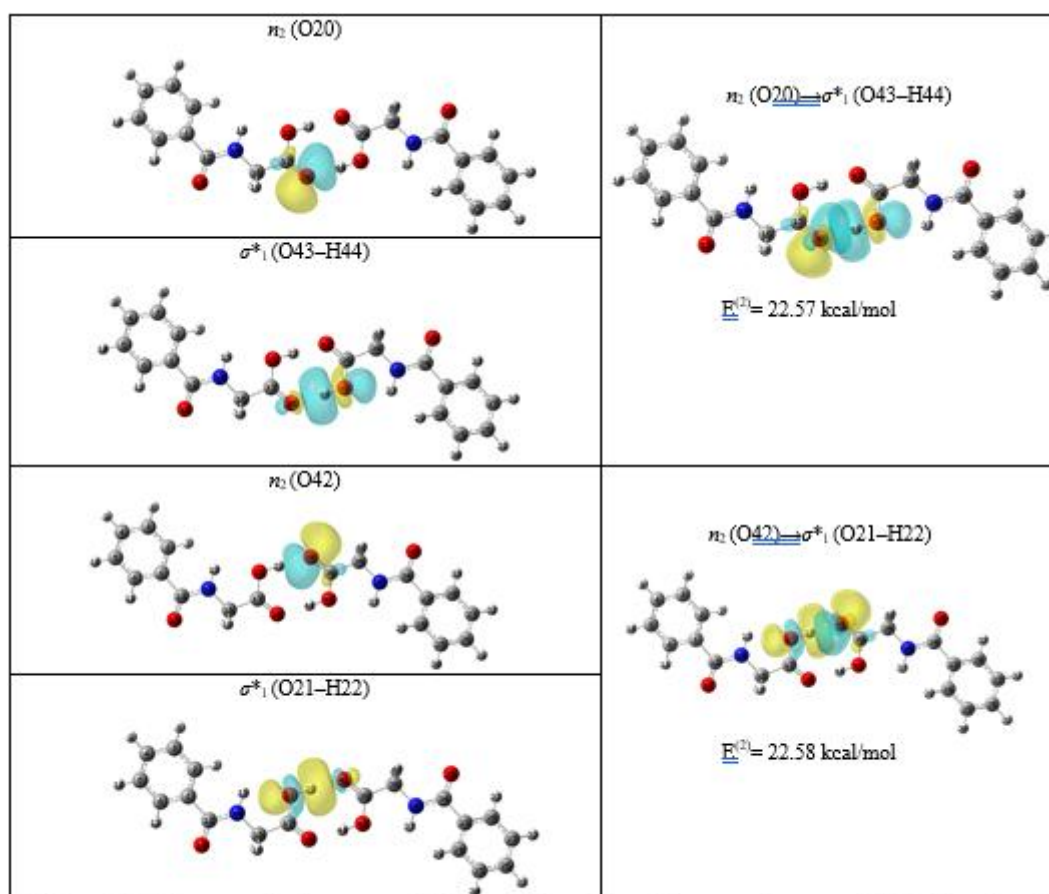


Figure 10: Electron density maps of O–H···O bonding of donor and acceptor NBOs involved in *inter*-molecular interactions of cyclic dimer structure of Hippuric acid.

The occupancies of the O–H···O bonded orbitals provide insights into the electron density distribution around specific atoms and their interactions. The unoccupied orbitals possess higher energies compared to the occupied orbitals. Descriptions of NBOs, along with their occupancies and H-bondings characteristics of CD1 structure are given in Table 8. The $\sigma(\text{O}21\text{--H}22)$ and $\sigma(\text{O}43\text{--H}44)$ orbitals are strongly polarized towards the H22 and H44 atoms, whereas the $\sigma^*(\text{O}21\text{--H}22)$ and $\sigma^*(\text{O}43\text{--H}44)$ orbitals are strongly polarized towards the O21 and O43 atoms. The natural hybrid on O21 is sp^2 hybridized, and natural hybrids on H22 have a completely sp character. The lone pair orbitals of oxygen atoms are sp hybridized with significant occupancy.

The lone pairs on $n_2(\text{O}20)$ and $n_2(\text{O}42)$, which initially had a significant 's' character (56.66%), shift towards a more 'p' character (reduced to 3.53%). The increased 'p' character in the lone pairs of O20 and O42, increases the electron density in regions that favor better overlap with the antibonding orbitals of the $\sigma^*(\text{O}21\text{--H}22)$ and $\sigma^*(\text{O}43\text{--H}44)$ bonds. The increased orbital overlap enhances the interaction between the oxygen lone pairs and the antibonding orbitals of the O–H bonds. As a result, there is a significant increase in the stabilization energies ($E^{(2)}$) of the H–bonds, from 9.37 kcal/mol to 22.57 kcal/mol, for both $n_2(\text{O}20)\rightarrow\sigma_1^*(\text{O}43\text{--H}44)$ and $n_2(\text{O}42)\rightarrow\sigma_1^*(\text{O}21\text{--H}22)$ interactions. The strength of the bonds can be calculated by examining the difference in occupancies between bonding and antibonding NBOs, represented as Δq . A larger Δq value generally indicates a stronger H–bond.

Table 8: Computed occupancy parameters for selected NBOs involved in O–H···O bonding within the cyclic dimer of Hippuric acid.

| NBOs $\Omega/\Omega^*(\text{A--B})$ | Occupancy q | Polarization coefficients (%) | | Description of NBO | Contribution of 's' character (%) | | Δq^* |
|--|------------------|-------------------------------|---------|--|-----------------------------------|-------|--------------|
| | | c_A^2 | c_B^2 | | A | B | |
| $\sigma(\text{O}21\text{--H}22)$ | 1.98468 | 78.88 | 21.12 | $0.8882(sp^{2.75})\text{O}21 + 0.4595(sp)\text{H}22$ | 26.64 | 99.77 | 1.91128 |
| $\sigma^*(\text{O}21\text{--H}22)$ | 0.07340 | 21.12 | 78.88 | $0.4595(sp^{2.75})\text{O}21 - 0.8882(sp)\text{H}22$ | | | |
| $\sigma(\text{O}43\text{--H}44)$ | 1.98468 | 78.88 | 21.12 | $0.8882(sp^{2.75})\text{O}43 + 0.4595(sp)\text{H}44$ | 26.64 | 99.77 | 1.91129 |
| $\sigma^*(\text{O}43\text{--H}44)$ | 0.07339 | 21.12 | 78.88 | $0.4595(sp^{2.75})\text{O}43 - 0.8882(sp)\text{H}44$ | | | |
| $n_1(\text{O}20)$ | 1.95580 | - | - | $sp^{0.76}$ | 56.66 | - | - |
| $n_2(\text{O}20)$ | 1.84501 | - | - | $sp^{27.33}$ | 03.53 | - | - |
| $n_1(\text{O}42)$ | 1.95580 | - | - | $sp^{0.76}$ | 56.66 | - | - |
| $n_2(\text{O}42)$ | 1.84500 | - | - | $sp^{27.32}$ | 03.53 | - | - |

Note: $^*\Delta q = q_{\Omega} - q_{\Omega^*}$

AIM and NCI analysis

Inter-molecular interactions in the CD1 structure are analyzed using AIM theory. According to AIM theory, O–H···O interactions are characterized by BCPs, bond paths and topological parameters, which provide insights into the strength and nature of the H–bonds^{21,22}. The CD1 structure involved the characterization of BCPs, which are graphically represented in Figure 11. Table 9 presents the topological parameters, such as electron density $\rho(r)$ and Laplacian of electron density, $\nabla^2\rho(r)$, for the H–bonding interactions of CD1 structure. The topological parameters at BCP indices 57 and 80 were found to be correlated with the H22···O42 and H44···O20 H–bonds. The values of $\rho(r)$ and the $\nabla^2\rho(r)$ for both H–bonds were determined as 0.05 and 0.1401 a.u. respectively. A positive value of $\nabla^2\rho(r)$ (0.1401) at both BCPs suggests a depletion of electron density along the bond paths of H22···O42 and H44···O20. The ratio of $-V(r)/G(r)$ is less than unity, where $G(r)$ and $V(r)$ represent the Lagrangian kinetic energy and potential energy densities, respectively. The total electronic energy density, $H(r)$, defined as the sum of $G(r)$ and $V(r)$, was evaluated at the BCPs. For the BCPs 57 and 80, the conditions $\nabla^2\rho(r) > 0$ and $H(r) < 0$ satisfy the criteria for existence of medium H–bond according to Rozas *et al*²³. Additionally, the interaction energy, E_{HB} , was determined to be 15.10 kcal/mol for both H–bonds.

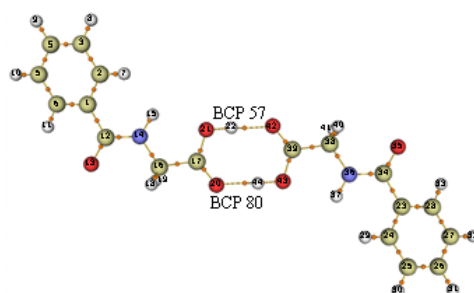


Figure 11: Molecular AIM graph for the CD1 structure of Hippuric acid. The bond critical points are represented by small orange spheres and numbers are representing BCP points.

Table 9: Topological parameters at selected BCPs for CD1 structure of Hippuric acid. All parameter magnitudes are in a.u., except interaction of H-bonding energy (E_{HB} , in kcal/mol).

| H-Bond Parameters | O21–H22···O42(57) | O43–H44···O20(80) |
|-------------------|-------------------|-------------------|
| $\rho(r)$ | 0.0500 | 0.0499 |
| $\nabla^2\rho(r)$ | 0.1401 | 0.1401 |
| $V(r)$ | -0.0481 | -0.0481 |
| $G(r)$ | 0.0416 | 0.0416 |
| $H(r)$ | -0.0065 | -0.0065 |
| E_{HB} kcal/mol | -15.1066 | -15.1066 |

Note: The numbers in the bracket, represent the bond critical points of H-bonding

NCI analysis was used to identify and visualize the nature and strength of interactions through color codes²⁴. The 2D and 3D NCI isosurface for the CD1 structure are shown in Figure 12. The blue patches (in Figure 12 (a)) between the hydrogen atom of C=O of COOH group of one monomer and oxygen atom of COOH group from another monomer represent the strong O–H···O (O21–H22···O42 and O43–H44···O20) bonds. In the RDG map, the H-bonds are represented by blue dots in the region of -0.04 to -0.05 a.u. of $\text{sign}(\lambda_2)\rho(r)$ values, indicating strong H-bonding. Green patches between the NH and OH groups within the monomer units represent van der Waals interactions in the cyclic dimer structure, while red patches indicate repulsive steric interactions. In the 2D map, the van der Waals interactions are predicted in the region of -0.01 to -0.02 a.u., and the steric interactions within the benzene ring correspond to positive $\text{sign}(\lambda_2)\rho(r)$ values, shown in red. The electron density maps and RDG maps indicate that the CD1 structure is strong H-bonded structure.

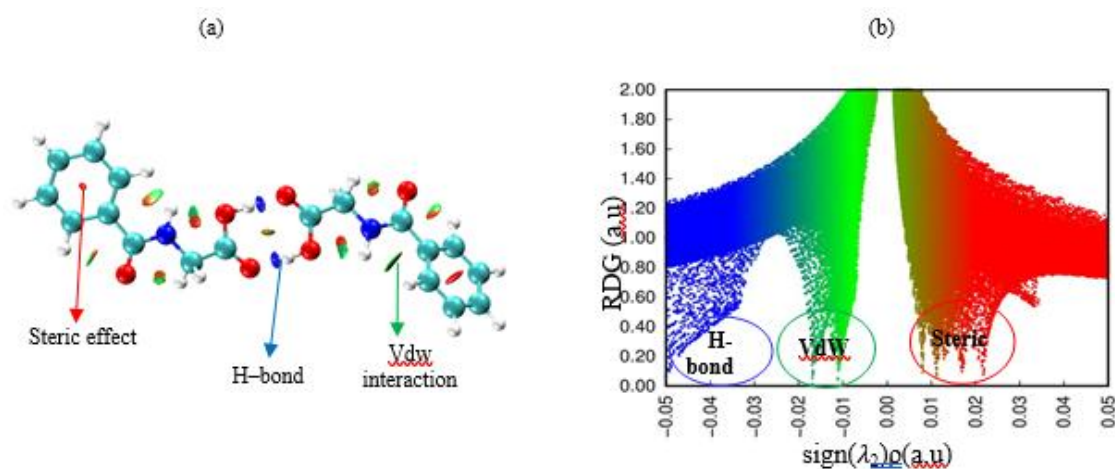


Figure 12: (a)- 3D visualization and (b)- 2D scatter plots of isosurfaces with isovalue = 0.5 au of RDG versus $(\text{sign } \lambda_2)\rho(r)$ for the cyclic dimer structure of Hippuric acid.

IV. Conclusion

In this chapter, we have studied different types of oligomer structures of Hippuric acid from MD simulations. After a simulation time of 10 ns in a water solvent, the final outcome contains linear dimer, cyclic dimer and trimer species. From $g(r)$ values for the H···O distances of the cyclic dimer species as obtained from the RDF, it has been found that the first prominent peak is within $r_c=2.72$ Å, confirming the existence of *inter*-molecular O–H···O bonding in oligomer structures. In all the dimer and trimer structures the most stable cyclic dimer structure is in good agreement with XRD data. The experimental IR spectrum produced a broad band structure with a peak at 3079 cm^{-1} due to multiple O–H···O bond interactions. The cyclic dimer structure has produced vibrational modes in very good agreement with the experimental data. We have also satisfactorily characterized the O–H···O interactions in the cyclic dimer structure in terms of NBO and AIM analysis. The interaction energies, E_{HB} of O–H···O bonds shows the strong H-bond; these results are consistent with the above NBO results.

References

- [1]. Karabacak M., Cinar Z., Mehmet C., A Structural And Spectroscopic Study On Para-Aminohippuric Acid With Experimental And Theoretical Approaches, *Spectrochim. Acta Part A*, 85(2012) 241-250. <https://doi.org/10.1016/J.Saa.2011.10.001>.
- [2]. Currie M., Hippuric Acid : A Neutron Diffraction Analysis, .C.S. Perkin II, 1974.
- [3]. Harrison W., Rettig S., And Trotter J., Crystal And Molecular Structure Of Hippuric Acid, *J.C.S. Perkin II*, 1972.

- [4]. Suresh Kumar B., Rajendra Babu K., Deepa M. And Vaidyan V. K., FT-IR Studies Of Pure And Doped Hippuric Acid Crystals, AIP Conference Proceedings 1075, (2008) 212. <https://doi.org/10.1063/1.3046216>.
- [5]. Alexander G. S., John F. And Bart K., Reversible Twisting During Helical Hippuric Acid Crystal Growth, J. AM. CHEM. SOC. 132, (2010) 9341–9349, <https://doi.org/10.1021/ja10149>.
- [6]. Refat M. S., Sabry A. El-Korashy, Ahmed S. A., Synthesis And Characterization Of Mn(II), Au(III) And Zr(IV) Hippurates Complexes, Spectrochim. Acta -Part A, 70 (2008) 840–849. <https://doi.org/10.1016/j.saa.2007.09.020>.
- [7]. Karabacaka M., Mehmet C., Mustafa Kurt, Molecular Structure And Vibrational Assignments Of Hippuric Acid: A Detailed Density Functional Theoretical Study, Spectrochim. Acta Part A 74 (2009) 1197–1203, <https://doi.org/10.1016/j.saa.2009.09.035>.
- [8]. Ringertz H., The Molecular And Crystal Structure Of Hippuric Acid, Acta Cryst. B27, (1971). 285.
- [9]. Bussi G., Donadio D., Parrinello M., Canonical Sampling Through Velocity Rescaling, J. Chem. Phys. 126 (2007) 014101. <https://doi.org/10.1063/1.2408420>
- [10]. Hoover W. Q., Ladd A. J. C. And Moran B., High-Strain-Rate Plastic Flow Studied Via Nonequilibrium Molecular Dynamics, Physical Review Letter, 48 (1982) 1818–20.
- [11]. Essmann Ulrich, Lalith Perera, Max L. Berkowitz, Tom Darden, Hsing Lee And Lee G. Pedersen, A Smooth Particle Mesh Ewald Method, J. Chem. Phys. 103 (1995), 8577–93. <https://doi.org/10.1063/1.470117>.
- [12]. Desiraju G. R. & Steiner T. The Weak Hydrogen Bond In Structural Chemistry And Biology, Oxford Univ. Press, Inc., New York, 2001.
- [13]. Colthup N.B., Daly L.H., Wiberley S.E., Introduction To Infrared And Raman Spectroscopy, Academic Press Inc, New York And London, 1964.
- [14]. Prabhu M.D., Tonannavar J., Tonannavar J., Multiple-H-Bonded-Zwitterionic Tetramer Structure For L-(+)-2-Chlorophenylglycine, As Investigated By UV, IR And Raman Spectroscopy And Electronic Structure Calculations, J. Mol. Struct. 1246 (2021). <https://doi.org/10.1016/j.molstruc.2021.131218>.
- [15]. Gilli G., Gilli P., The Nature Of The Hydrogen Bond, Oxford University Press, 2009.
- [16]. Ramanna P., J. Tonannavar, J. Tonannavar, Study Of H-Bonded Cyclic Dimer Of Organic Linker 5-Bromoisophthalic Acid By DFT And Vibrational Spectroscopy, J. Mol. Struct. 1241 (2021), 130613, <https://doi.org/10.1016/j.molstruc.2021.130613>.
- [17]. Bellamy L.J., The Infra-Red Spectra Of Complex Molecules, Third Ed., Chapman And Hall, London, 1975.
- [18]. Socrates G., Infrared Characteristic Group Frequencies, John Wiley And Sons, New York, London, Sydney, Toronto, 1980.
- [19]. Weinhold F., Reed A.E., Curtiss L.A., Intermolecular Interactions From A Natural Bond Orbital, Donor—Acceptor Viewpoint, Chem. Rev. 88 (1988) 899–926. <https://doi.org/10.1021/cr00088a005>.
- [20]. Pallavi L., Tonannavar J., Tonannavar J., Molecular Dynamics Simulations, DFT Calculations And Vibrational Spectroscopic Study Of N-H···O Bound Dimer Models For DL-B-Phenylalanine And 3-Amino-3-(4-Chlorophenyl)Propionic Acid, J. Mol. Liq. (2022) 352, <https://doi.org/10.1016/j.molliq.2022.118746>.
- [21]. Bader R.F.W., A Quantum Theory Of Molecular Structure And Its Applications, Chem. Rev. 91 (1991) 893–928, <https://doi.org/10.1021/cr00005a013>.
- [22]. Popelier P.L.A., Characterization Of A Dihydrogen Bond On The Basis Of The Electron Density, J. Phys. Chem. A 102 (1998) 1873–1878, <https://doi.org/10.1021/jp9805048>.
- [23]. Rozas, I. Alkorta, J. Elguero, Behavior Of Ylides Containing N, O, And C Atoms As Hydrogen Bond Acceptors, J. Am. Chem. Soc. 122 (2000) 11154–11161.
- [24]. Johnson E.R., Keinan S., Mori-Sanchez P., Contreras-García J., Cohen A.J., Yang W., Revealing Noncovalent Interactions, J. Am. Chem. Soc. 132 (2010) 6498–6506.